communications earth & environment

Article

https://doi.org/10.1038/s43247-024-01274-1

The risk of concurrent heatwaves and extreme sea levels along the global coastline is increasing

Mo Zhou[1] & Shuo Wang[1,2] ✉

Concurrent heatwaves and extreme sea levels could pose a serious threat to coastal communities under climate change; however, the spatiotemporal characteristics and dynamic evolution of them along global coastline remain poorly understood. Here, we use reanalysis datasets and model projections to assess historical and future changes in global concurrent heatwaves and extreme sea levels. We find that 87.73% of coastlines experienced such concurrent extremes during 1979–2017. There is an average increase of 3.72 days in the occurrence during 1998–2017 compared to 1979–1998. A one-percentile increase in heatwave intensity is associated with a 2.07% increase in the likelihood of concurrent extremes. Global coastlines are projected to experience 38 days of concurrent extremes each year during 2025–2049 under the highest emission scenario. The weakening of geopotential height associated with a surface low-pressure system may serve as an important indicator for the occurrence of extreme sea levels during heatwaves.

Coastal areas are the frontlines of climate change[1–3]. Both heatwaves over land and extreme sea levels pose a serious threat to coastal communities in the face of climate change[4–7]. Global and regional studies demonstrate that the increasing heatwaves have resulted in, and will continue to result in, severe socioeconomic and ecological consequences in a changing climate[8–13]. For example, the 2006 California heatwave resulted in over 600 deaths, disproportionately affecting densely populated coastal areas[8,14]. Coastal communities are also periodically exposed to extreme sea levels[15], which result from the combination of storm surges and high astronomical tides. And extreme sea levels are expected to increase even further due to the long-term rise in sea levels[16,17]. Extreme sea levels can cause coastal flooding when flood defenses are overtopped, threatening life and property in coastal communities[5]. It is estimated that on average 0.8–1.1 million people per year around the world are affected by coastal flooding[18]. The high vulnerability of affected areas to heatwaves and extreme sea levels can also exaggerate their dangers, as global population and economic activity tend to concentrate in low-lying coastal areas[19].

Concurrence of heatwaves and extreme sea levels (CHWESL) in the same location constitutes an emerging compound event that could lead to larger impacts than the sum of impacts due to individual hazards striking alone. Specifically, CHWESL events can pose unexpected flooding and drowning risks, posing a threat to coastal residents and tourists during heatwaves. An example of this phenomenon occurred in August 2021: extreme sea level-induced flooding struck the Mediterranean region while local temperatures reached approximately 50 °C[20,21]. In addition, acting as different stressors, concurrent heatwaves and extreme sea levels may exceed the coping capacity of an affected system like other compound events[22]. Despite the substantial impacts, CHWESL events have received far less attention compared to other types of compound events. There is currently a lack of global picture of CHWESL dynamics and evolution in response to the changing climate. The physical mechanisms behind CHWESL events also remain unclear. Thus, there is an urgent need for a comprehensive assessment of CHWESL events from a global perspective, particularly given the projected increases in both the intensity and frequency of heatwaves and extreme sea levels[16,22,23] as well as the projected growth of coastal population and urbanization[24–26].

In this study, we aim to provide an in-depth assessment of historical patterns and future changes in the characteristics of concurrent heatwaves and extreme sea levels on a global scale, based on reanalysis datasets and Coupled Model Intercomparison Project Phase 6 (CMIP6) projections. We will also investigate the sensitivity of CHWESL events to the intensity of individual extremes and the underlying mechanisms of such extreme events. This study will not only contribute to a deeper understanding of the emerging type of compound extremes (CHWESL events), but also provide crucial insights into the implementation of adaptation and early warning systems that can help mitigate the negative consequences of such extreme events.

[1]Department of Land Surveying and Geo-Informatics, The Hong Kong Polytechnic University, Hong Kong, China. [2]Research Institute for Land and Space, The Hong Kong Polytechnic University, Hong Kong, China. ✉e-mail: shuo.s.wang@polyu.edu.hk

Results

Characteristics of concurrent heatwaves and extreme sea levels

The occurrence of CHWESL events is defined as the number of CHWESL days within a year. Using extreme sea levels derived from the ERA5 reanalysis dataset (ESL reanalysis), we calculated the total occurrence of CHWESL events during 1979–2017. Most of the coastlines (87.73%) have been affected by CHWESL events during the period of 1979–2017, with a concentration of these events in the tropical region (Fig. 1a). Specifically, tropical coastlines, which account for only 47.09% of the total coastal area, have experienced 70.30% of all CHWESL events worldwide. For each grid cell in the tropical region, the average total occurrence of CHWESL events is 75 days during 1979–2017. In contrast, subtropical and temperate zones show a lower occurrence of CHWESL for only 39 and 11 days, respectively. Results derived from the GESLA observation dataset (ESL observation) support the same finding that lower-latitude regions are more prone to CHWESL events (Supplementary Fig. 2c–d).

To assess whether the occurrence of CHWESL events is purely a coincidence, we used a bootstrap-resampling-based significance test[27] to generate random CHWESL events and compared these with the detected CHWESL events based on the ERA5 reanalysis dataset (see Supplementary Methods and Supplementary Fig. 4). The total occurrence of detected CHWESL events is significantly higher than the CHWESL events expected due to random coincidence at a 95% confidence level. Assuming heatwaves and extreme sea levels are concurrent by chance, the average total occurrence of CHWESL events would drop from 41 days to 23 days. This indicates that the interaction between heatwaves and extreme sea levels contributes an additional 78.26% to the total occurrence of CHWESL events.

We divided the period from 1979 to 2017 into two 20-year periods (1998–2017 and 1979–1998) and calculated the changes in the occurrence of CHWESL events during these two periods. Our findings indicate that 39.12% of the world's coastal areas have experienced a significant increase in the occurrence of CHWESL events in recent 20 years, with an average increasing occurrence of 3.72 days (Fig. 1c). Lower-latitude regions, such as West Africa (WAF), Southeast Asia (SEA), East Africa (EAF), and the Pacific Islands Region (PIR), show a more pronounced increase in the occurrence of CHWESL events (Fig. 1d).

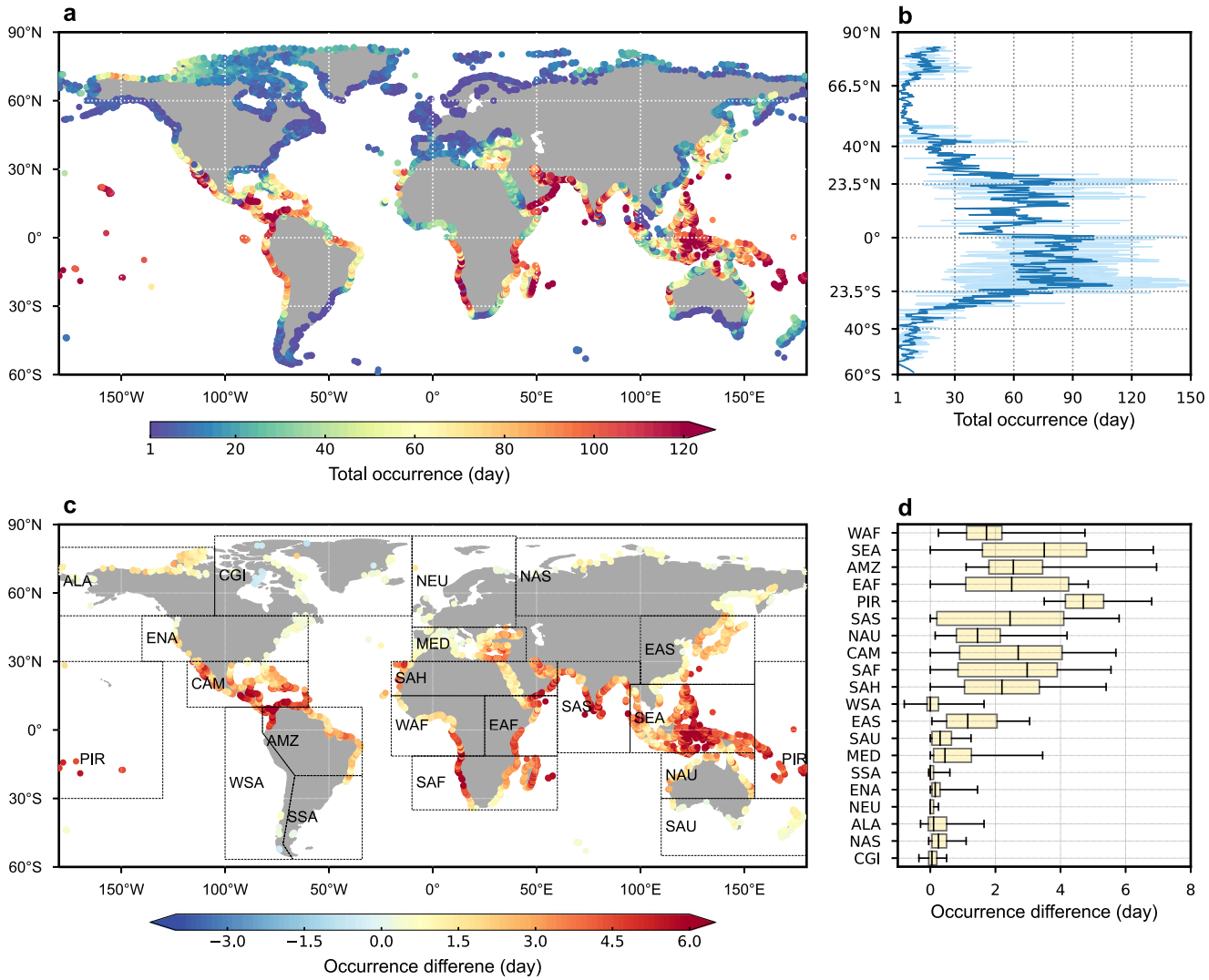

Fig. 1 | Characteristics of CHWESL events during 1979–2017. a Total occurrence (day) of CHWESL events during 1979–2017. **b** Total occurrence (day) of CHWESL events for grid cells at different latitudes. The shading spans an anomaly of ±1 s.e.m. To enable comparisons between grid cells at different latitudes, the total occurrence of all grid cells is averaged for each latitude. **c** Differences in the CHWESL occurrence (day) between 1998–2017 and 1979–1998. Statistical significance of the difference is estimated by the Student's *t* test at a 95% confidence level. Grid cells with insignificant differences are excluded from the change analysis. **d** Occurrence difference (day) for each divided region. Each box represents the distribution of occurrence difference across all grid cells within that region. The box is bounded by the 25th and 75th percentiles of the data, and the whisker is bounded by the 5th and 95th percentiles of the data. The order of coastal regions is determined by the average latitude of each region.

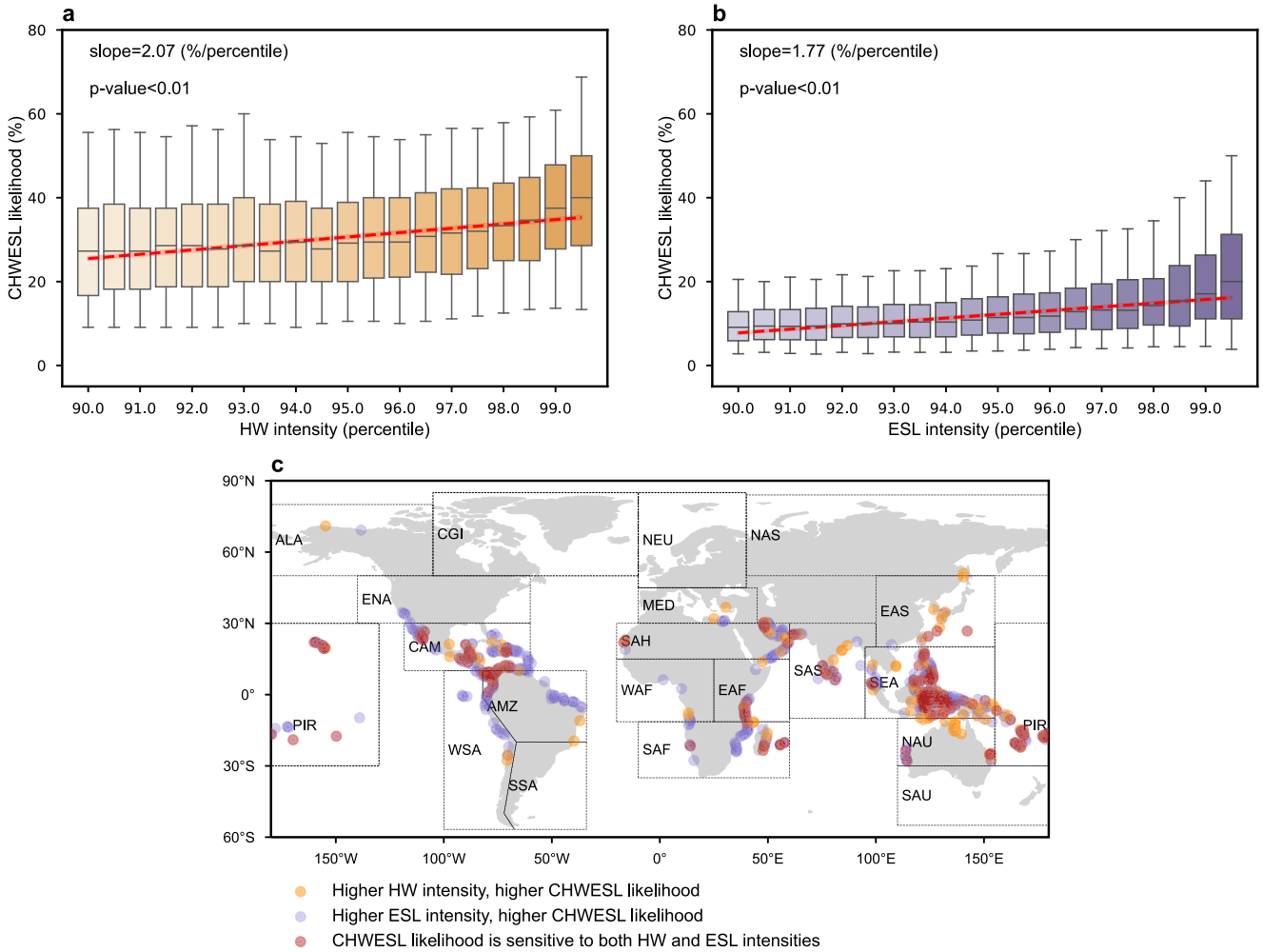

Fig. 2 | Sensitivity of CHWESL events to the intensity of individual extremes. **a** Changes in the likelihood of CHWESL events during heatwaves with increasing intensities. Intensity of a heatwave day is determined by the percentile of the equivalent temperature on that day. We have defined 20 levels of intensity ranging from the 90th to the 99.5th percentile, with an interval of 0.5th percentile. Heatwaves with a 90th intensity refer to those where the equivalent temperature on that day is equal to or greater than the 90th percentile but less than the 90.5th percentile. Boxplots show the distribution of CHWESL likelihood during heatwaves with a specified intensity across all grid cells. Boxes in the boxplot are bounded by the 25th and 75th percentiles of the data, and the whiskers represent the 5th and 95th percentiles of the data. The red dashed line represents the fitted linear regression between the heatwave intensity (x-axis) and the median values of CHWESL likelihood (y-axis). **b** Same as **a** but CHWESL likelihood is calculated during extreme sea levels with increasing intensities. Intensity of an extreme sea level day is determined by the percentile of the total water level on that day. **c** Sensitivity of CHWESL likelihood to the intensity of heatwaves (yellow) and extreme sea levels (purple) for each grid cell. Grid cells where the CHWESL likelihood shows significant sensitivity to the intensities of both heatwaves and extreme sea levels will be marked in red. Grid cells with insignificant trends are excluded from the sensitivity analysis.

Sensitivity of CHWESL events to the intensity of individual extremes

Given that regions with a higher risk of CHWESL events are primarily concentrated in the tropical region, which is typically characterized by hotter and more humid conditions, we hypothesize that these conditions may be associated with the occurrence of CHWESL events. To test this hypothesis, we conducted sensitivity experiments by categorizing heatwaves into 20 levels based on their intensities and examined the likelihood of CHWESL events during heatwaves with varying intensities. The intensity of a heatwave day is determined by the percentile of the equivalent temperature on that day. Equivalent temperature is derived from air temperature and specific humidity. Therefore, a higher intensity indicates higher air temperature and higher specific humidity, corresponding to hotter and more humid conditions, respectively. The likelihood of CHWESL events during heatwaves of a specific intensity is determined by calculating the ratio between the number of heatwave days that are concurrent with extreme sea levels (i.e., CHWESL events) and the total number of heatwave days with that specific intensity.

Generally, our findings indicate a significant increase in the likelihood of CHWESL events as heatwaves become more intense (Fig. 2a and Supplementary Fig. 7a). On average, a one-percentile increase in heatwave intensity corresponds to a 2.07% increase in the likelihood of heatwaves that are concurrent with extreme sea levels. Specifically, we observed that 16.67–37.50% of heatwaves with the 90.0th percentile intensity is concurrent with extreme sea levels, while this likelihood increases to 28.57–50.00% for heatwaves with the 99.5th percentile intensity. These findings suggest that more intense heatwaves, characterized by higher air temperature and higher specific humidity, are more likely to occur simultaneously with extreme sea levels, thereby amplifying the risk of CHWESL events. This is particularly concerning considering that heatwaves with the 99.5th intensity are already unbearable for coastal communities. Additionally, we calculated the absolute number of CHWESL days during heatwaves with varying intensities (Supplementary Figs. 6a and 7c). Our analysis reveals a notable increase in the number of CHWESL days as heatwaves become more intense. This verifies our findings that more intense heatwave could amplify the risk of CHWESL events.

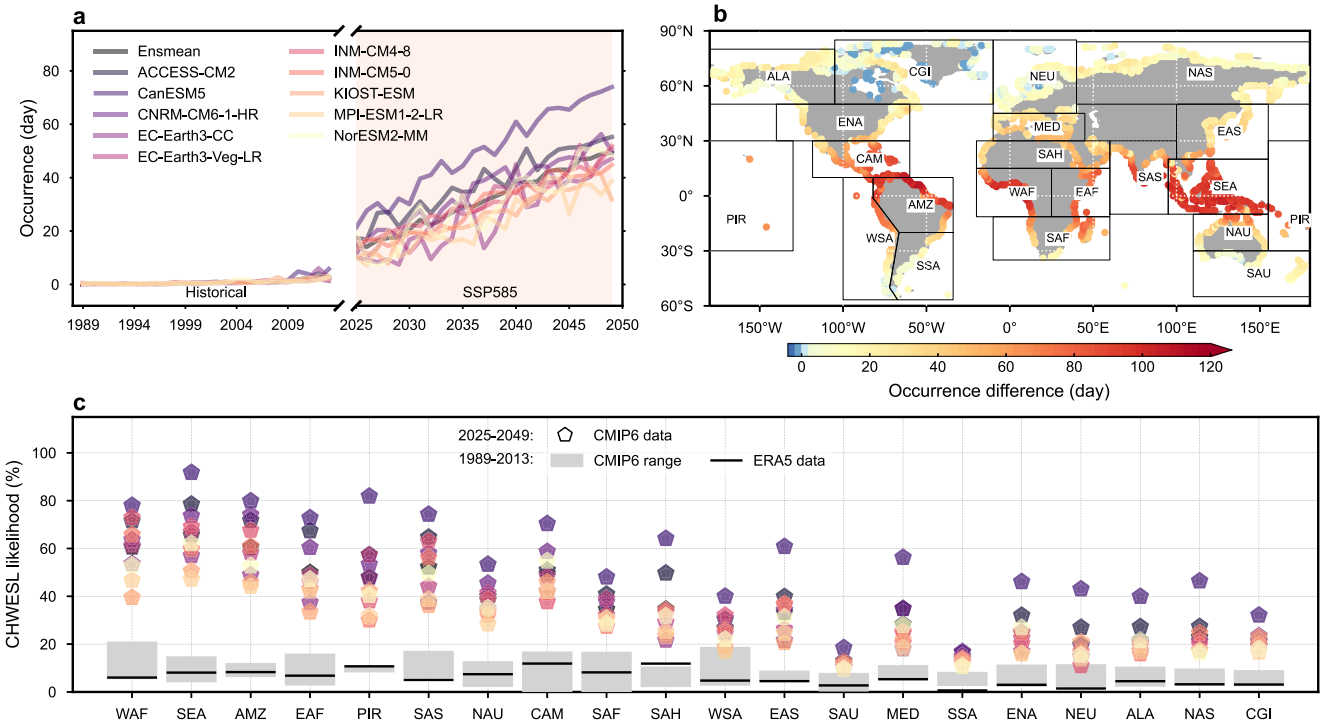

Fig. 3 | Projected changes in the characteristics of CHWESL events. a Occurrence (day) of CHWESL events during the future period of 2025–2049 and the historical period of 1989–2013 based on 10 CMIP6 simulation models. **b** Average differences in the CHWESL occurrence (day) between the future period (2025–2049) and the historical period (1989–2013) across 10 CMIP6 simulation models. For each simulation model, the statistical significance of the difference is estimated by the Student's *t* test at a 95% confidence level. Only grid cells that exhibit a significant difference across all 10 CMIP6 simulation models are included in the change analysis. **c** Likelihood of CHWESL events for each coastal region during the historical and future periods. The stars represent the average likelihood of CHWESL events during the future period in each region. The 10 stars represent the 10 CMIP6 simulation models. The gray shading illustrates the 95% uncertainty range of CMIP6 historical simulations. The lower and upper bounds of the gray shading represent the 2.5th and 97.5th percentile estimates of the likelihood of CHWESL events across the 10 CMIP6 models, respectively. The black line is the likelihood of CHWESL events identified based on ERA5 reanalysis data during the same historical period of 1989–2013. The order of coastal regions is determined by the average latitude of each region.

We also examined the sensitivity of the likelihood of CHWESL events to the intensity of extreme sea levels (Fig. 2b and Supplementary Fig. 7b), using analogous percentile-based intensities. This likelihood was determined by calculating the ratio between the number of extreme sea level days that are concurrent with heatwaves and the total number of extreme sea level days at a specific intensity. We find that the likelihood of CHWESL events increases by 1.77% when the intensity of extreme sea levels increases by one percentile. This implies that both more intense heatwaves and more intense extreme sea levels can increase the likelihood of CHWESL events. Notably, SEA, EAF, PIR, and the Central America and Mexico (CAM) are particularly exposed to the synergistically amplified risk (Fig. 2c). The results obtained from the ESL observation consistently demonstrate the sensitivity of CHWESL events to the intensity of two individual extremes, as shown in Supplementary Fig. 5c, d. These synergistic amplification effects are further evident in the correlation between the intensities of heatwaves and extreme sea levels (Supplementary Fig. 8).

Future projection of CHWESL events

To assess the potential impacts of climate change on CHWESL events, we projected the occurrence of CHWESL events during the future period of 2025–2049 under the SSP585 scenario based on an ensemble of the Coupled Model Intercomparison Project Phase 6 (CMIP6) model outputs. Our findings reveal that global coastal communities are expected to experience 38 days of CHWESL events each year during the future period of 2025–2049, representing an average increase of 31 days compared to the historical period of 1989–2013 (Fig. 3a, b). This increase is primarily attributed to a warming climate under the highest-emission scenario (SSP585). Particularly, the tropical coastal regions, such as WAF, SEA, and Amazon (AMZ), witness the strongest increase in the occurrence of CHWESL events (Fig. 3b and Supplementary Fig. 10). These findings imply that coastal communities will face a disproportionably increasing risk of CHWESL events, with tropical regions facing the most serious threat from such a concurrent extreme.

The projected increase in the likelihood of CHWESL events during heatwaves is statistically significant and most climate models agree on the changes in each region (Fig. 3c and Supplementary Fig. 14). On average, the likelihood of global CHWESL events during the future period is projected to increase by fivefold compared to the historical period. This increase is particularly prominent in lower-latitude coastal regions. For instance, in SEA, the likelihood of CHWESL events is expected to be up to eight times higher than that in the historical period. This indicates that under a warmer climate, heatwaves are more likely to be concurrent with extreme sea levels, which is consistent with our findings that hotter and more humid heatwaves may amplify the risk of CHWESL events.

Atmospheric conditions associated with CHWESL events

The days experiencing heatwaves and extreme sea levels were categorized into three groups, including CHWESL days, heatwave days that are not concurrent with extreme sea levels (referred to as "HWN days"), and extreme sea level days that are not concurrent with heatwaves (referred to as "ESLN days"). We used the composite of large-scale atmospheric variables[28,29] to disentangle the influence of atmospheric conditions on CHWESL events (Supplementary Figs. 15–17).

The CHWESL days along the global coastline are characterized by simultaneous warm temperature anomalies (Supplementary Fig. 15b) and high sea level anomalies (Supplementary Fig. 15e), similar to what is observed during HWN days (Supplementary Fig. 15a) and ESLN days (Supplementary Fig. 15f), respectively. Corresponding to warm temperature

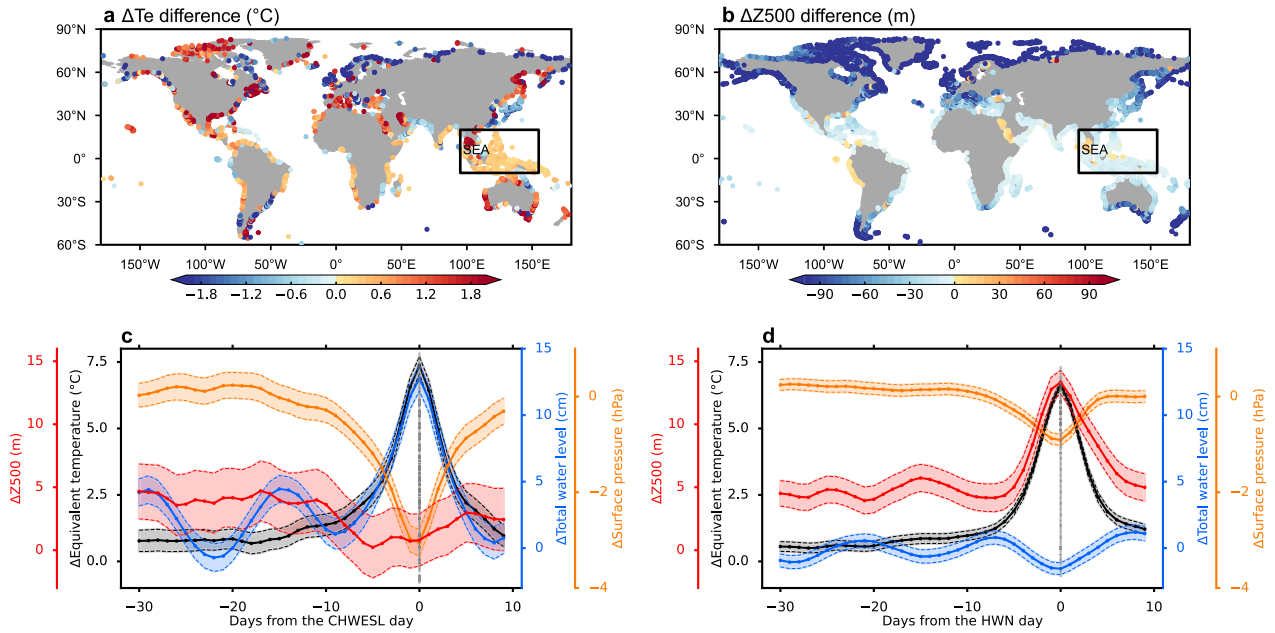

Fig. 4 | Anomalies of atmospheric variables during CHWESL days and HWN days. a Difference in the anomalies of equivalent temperature (ΔT_e) during CHWESL days and HWN days. The statistical significance of the difference is estimated by the Student's *t* test at a 95% confidence level. Grid cells with insignificant differences are excluded from the difference analysis. **b** Same as **a** but for the difference in the anomalies of geopotential height (ΔZ500). **c** Evolution of anomalies in atmospheric variables from 30 days before the CHWESL day to 10 days after the CHWESL day in the SEA region. **d** Evolution of anomalies in atmospheric variables from 30 days before the CHWESL day to 10 days after the HWN day in the SEA region.

anomalies, both CHWESL days and HWN days are characterized by elevated geopotential height at 500 Pa (Z500) (Supplementary Fig. 16a, b) and increased surface solar radiation (Supplementary Fig. 16d, e). The high Z500 in the atmosphere is typically linked to anticyclonic systems generating warm air, and the heightened surface solar radiation supplies abundant energy for land surface heating[30,31]. Despite the equivalent temperature anomalies during CHWESL days are comparable to, and even higher than, those during HWN days along most coastlines (Fig. 4a), we observe lower Z500 values during CHWESL days (Fig. 4b).

Through the analysis of the evolution of atmospheric variables in the SEA region during the 30 days prior to the CHWESL day (Fig. 4c) and the HWN day (Fig. 4d), we find that the discrepancy in Z500 between CHWESL days and HWN days can be attributed to the different evolution of Z500 prior the CHWESL day and HWN day. Specifically, there is a decreasing trend in Z500 starting from 10 days prior to the CHWESL day, accompanied by an obvious decrease in surface pressure (Fig. 4c). Surface pressure continuously decreases during that time, reaching its lowest value on the CHWESL day. This indicates that the blocking highs responsible for generating warm air are weakening before the CHWESL day and transitioning into a surface low-pressure system. In contrast, Z500 exhibits a significant increasing trend from 10 days prior to the HWN day. On the HWN day, Z500 reaches its peak and surface pressure remains relatively stable. These results indicate that the distinct evolution of Z500 before the CHWESL day and the HWN day may be closely linked to the variations in surface pressure.

This low surface pressure during CHWESL days (Supplementary Fig. 17b) resembles what is observed during ESLN days (Supplementary Fig. 17c). Such a surface low-pressure system is often observed during tropical cyclones or other intense weather systems[32,33], and it can contribute to the generation of strengthening winds[34] (Supplementary Fig. 17e, f). These winds can trigger storm surges by driving water towards the coast. Therefore, the combination of a surface low-pressure system, intensifying winds, and the resulting storm surge can elevate total water levels, leading to extreme sea levels[35]. Our findings indicate that the weakening of blocking highs and their transition into a surface low-pressure system may serve as important indicators for the occurrence of CHWESL events. Supplementary Fig. 18 illustrates the same analysis of atmospheric variable evolution for the regions of EAF and PIR, and the results align with our findings.

Discussion and conclusions

The climate-induced heatwave and extreme sea level have been receiving increasing attention in recent years due to their adverse effects on coastal communities, but they are usually treated individually. This study provides a comprehensive investigation of concurrent heatwave and extreme sea level events along the global coastline. We identified global hotspots of CHWESL events and explored their dynamic evolution in response to the warming climate. We also examined the sensitivity of the likelihood of CHWESL events to the intensity of individual extremes. In addition, we investigated the potential physical processes linked to the occurrence of CHWESL events.

Our findings reveal that the global coastline experienced a significant increase in the occurrence of CHWESL events during the period of 1979–2017. Coastlines in the tropical region are at higher risk for CHWESL events, as evidenced by both a higher occurrence of CHWESL events and a larger occurrence differences between two 20-year periods. Furthermore, we find that hotter and more humid heatwaves are more likely to be concurrent with extreme sea levels globally. More intense heatwaves and more intense extreme sea levels may synergistically increase the likelihood of CHWESL events in SEA, EAF, and PIR. Under the highest emission scenario of SSP585, the global coastline is expected to experience a higher occurrence and a higher likelihood of CHWESL events. Weakening of geopotential height at 500hPa accompanied by the emergence of a surface low-pressure system may serve as crucial indicators for CHWESL events.

The evolution of CHWESL events varies across global coastal areas. Approximately 39.12% of the global coastline experienced a significant increase in the CHWESL occurrence in recent 20 years, whereas there is a significant decrease of CHWESL events in Canada, Greenland, and Iceland (CGI) and the West Coast of South America (WSA). The decreasing CHWESL events in CGI corresponds to the decreasing extreme sea levels (Supplementary Fig. 3d), which is due to the fact that the land beneath the

ice sheet rises in this region as the substantial weight of ice sheet is removed when Greenland losing ice under a warmer climate[36]. And the decreasing CHWESL events in WSA is due to the decreasing humid heatwave (Supplementary Fig. 3b). This agrees with the results of previous studies[37,38]. Nevertheless, the WSA is expected to experience increasing CHWESL events during the future period of 2025–2049. Thus, coastal communities without emergency response systems may face a significant threat from the increasing CHWESL occurrence in the future.

Our study primarily focused on the highest emission scenario to evaluate the potential risks and impacts of CHWESL events. We recognize that different emission scenarios can lead to varying outcomes. In more optimistic emission scenarios, characterized by stronger mitigation efforts and reduced greenhouse gas emissions, it is plausible to expect a decrease in the frequency and intensity of CHWESL events. Future research that explores alternative emission scenarios and their effects on CHWESL events would be valuable in providing a comprehensive understanding of the full range of potential outcomes.

The atmospheric conditions associated with CHWESL events suggest that a weakening anticyclonic circulation and a simultaneous surface low-pressure system may contribute to extreme sea levels during heatwaves. These low-pressure systems, which induce extreme sea levels, are often considered important features of tropical cyclones[32,33]. Previous studies have suggested that anomalous warm and humid conditions can precede the occurrence of tropical cyclones, as these cyclones can modulate atmospheric circulations and trigger anomalous descending motion[39–41]. As a result, hot weather conditions can persist until the tropical cyclones make landfall. It is worth noting that surface pressure can decrease several days before the landfall of a tropical cyclone, even if the hot conditions are still ongoing[41]. Therefore, it is reasonable to consider the potential overlap between ongoing heatwaves and upcoming extreme sea levels, as these two phenomena may be interconnected. However, the interactions between land and ocean environments are rather complex. Further research and investigations are necessary to fully understand and unravel the underlying physical mechanisms that govern the occurrence of CHWESL events.

The CHWESL event could pose a significant threat to coastal communities in terms of beach activities and power supply. On the one hand, individuals who seek relief from hot weather by engaging in beach activities may potentially increase their exposure to extreme sea levels during heatwaves. Low- and middle-income countries, such as Indonesia and Mexico, are particularly vulnerable to such a risk since the majority of households do not have access to space-cooling devices to alleviate the effects of hot weather[42,43]. On the other hand, even in high-income countries where air conditioners are more widely available during heatwaves, the flooding caused by extreme sea levels can disrupt power supplies[44], worsening the existing thermal risks.

The potential impacts of CHWESL events for each region are also determined by a combination of the characteristics of extreme events and the inherent vulnerabilities of the region. Approximately 40% of the world's population (3 billion people) is living in the tropics[45] where are the hotspots of CHWESL events and are already experiencing the highest temperatures and greatest sea-level rise[46,47]. Countries located in the tropics are major contributors to global population growth[48,49], which can further increase exposure risk and exacerbate the vulnerability of communities in these regions to CHWESL events. Moreover, people living in low-lying islands in the tropics, such as those in the Caribbean, Pacific, and Southeast Asia (i.e., CAM, PIR, and SEA) are far more likely to be harmed by CHWESL events. This is due to many people living there have low- or middle-income and reside in developing countries[49]. CHWESL events could impose more adverse impacts on developing countries due to a lack of adaptive capacity[50]. Our findings indicate that there is a pressing need to inform adaptation planning of CHWESL events in the tropics. Therefore, this study is crucial in advancing our understanding of the evolution and mechanisms of CHWESL events along the global coastline, as well as in developing effective risk mitigation strategies.

Data and methods

Data

We used daily maximum 2-m air temperature, daily mean 2-m dew point temperature, and daily mean surface pressure from the daily ERA5 reanalysis dataset[51,52] to calculate the equivalent temperature (T_e, °C), and then to identify heatwave events. Large-scale atmospheric variables were also retrieved from the ERA5 reanalysis dataset, including geopotential height at 500 hPa, surface solar radiation, surface pressure, and 10-m u-component of wind and v-component of wind. The dataset has a spatial resolution of 0.25° and covers a 39-year period from 1979 to 2017.

We used total water level derived from the ERA5 reanalysis dataset and tide gauge observations to identify extreme sea levels. The ERA5 reanalysis total water level[43] provides globally homogenized water level data for the period from 1979 to 2017. This reanalysis total water level is simulated based on the hydrodynamic model (Deltares Global Tide and Surge Model version 3.0) using climate forcing from the ERA5 global reanalysis. It is characterized by temporal stability, temporal continuity (no gaps or missing values), and spatial continuity for it covers almost all the global coastline. Specifically, it has a temporal resolution of 10-minute and was aggregate to daily mean total water level (Wt, cm) to identify extreme sea levels. It includes sea stations with a spatial resolution of 0.1° in the near coastal area and 0.25° in the ocean area within 100 km of the coastline.

To validate the results obtained from the ERA5 reanalysis dataset regarding extreme sea levels, we collected tide gauge observations from the Global Extreme Sea Level Analysis (GESLA) 3 dataset[44–46]. For our analysis, we only considered tide gauges that had a minimum of 20 years of observations within the study period of 1979–2017. This selection process resulted in a total of 864 tide gauges that were used for further analysis. To ensure consistency, we aggregated the hourly tide gauge observations into daily mean total water level. Approximately 40% of these 864 tide gauges provided data spanning more than 35 years of total water level observations. The spatial distribution of these selected tide gauges is shown in Supplementary Fig. 21, which illustrates their concentration along the coastlines of Europe, Japan, America, Canada, and Australia.

All projection datasets used in this study are based on CMIP6 climate projections under the SSP585 emission scenario for the future period of 2025–2049. Multiple CMIP6 models were selected based on data availability and good performance in simulating meteorological variables to minimize the uncertainty originating from datasets[53]. Simulated 2-m air temperature and specific humidity used to calculate the equivalent temperature under global warming are based on 10 bias-corrected CMIP6 climate projections, including ACCESS-CM2, CanESM5, CNRM-CM6-1-HR, EC-Earth3-CC, EC-Earth3-Veg-LR, INM-CM4-8, INM-CM5-0, KIOST-ESM, MPI-ESM1-2-LR, and NorESM2-MM[54]. The simulated total water level is based on five bias-corrected CMIP6 climate projections, including CMCC-CM2-VHR4, EC-Earth3P-HR, GFDL-CM4C192-SST, HadGEM3-GC31-HM, and HadGEM3-GC31-HM-SST[55]. All simulation datasets were gridded to 1° spatial resolution using the bilinear interpolation method. The reason for the inconsistent selection of climate projections for equivalent temperature and total water level is the absence of a single climate projection that encompasses both variables. In this study, we identified CHWESL events based on heatwaves derived from 10 CMIP6 simulation models of equivalent temperature and extreme sea levels derived from the ensemble mean of five CMIP6 simulation models of total water level (Fig. 3 and Supplementary Fig. 10). We also detected CHWESL events based on heatwaves derived from the ensemble mean of 10 CMIP6 simulation models of equivalent temperature and extreme sea levels derived from five CMIP6 simulation models of total water level, as shown in Supplementary Figs. 11 and 12. The historical period (1989–2013) was used as a reference to analyze future changes in CHWESL events. We verified the capacity of CMIP6 models to capture the characteristics of CHWESL events by reproducing historical CHWESL events[56,57] (Supplementary Methods and Supplementary Fig. 13). Since the projected equivalent temperature is based on 10 CMIP6 models and the projected total water level is based on five CMIP6 models, we employed an ANOVA-based variance decomposition

method to partition the total uncertainty in the projected changes of CHWESL events (Supplementary Methods and Supplementary Fig. 22).

The global coastline was derived from the Global Self-consistent, Hierarchical, High-resolution Geography database (GSHHG)[58]. The GSHHG is a high-resolution geography dataset amalgamated from three databases in the public domain, including World Vector Shorelines (WVS), CIA World Data Bank II (WDBII), and Atlas of the Cryosphere (AC), and has been widely used in coastal studies[59,60]. We utilized the reference regions of the Fifth Assessment Report of the United Nations Intergovernmental Panel on Climate Change AR5 (IPCC AR5)[61,62] with minor modifications to examine the details of regional coastlines (Supplementary Fig. 1). The order of coastal regions (Fig. 1d and Fig. 3c) was determined by the average latitude of each region. The area of each grid cell is estimated using the area of equatorial grid cell weighted by the cosine of its latitude, to account for the different sizes of grid cells between different latitudinal zones due to the convergence of lines of latitude towards the poles[63,64]. We defined the daily anomalies by subtracting the seasonal cycle, which is the day-of-year mean for each meteorological variable (e.g., 1979–2017)[41].

Calculation of equivalent temperature

In this study, we used equivalent temperature (T_e) to investigate heatwaves along the global coastlines as it can effectively capture changes in both air temperature and humidity. This responds to a recent demand to account for the influence of humidity on heat, as the equivalent temperature is a more accurate measurement of thermal discomfort[65]. The T_e is derived from the moist static energy (H) and calculated as:

$$T_e = \frac{H}{C_p} = T + \frac{L_v q}{C_p} \tag{1}$$

where C_p is the specific heat of air at constant pressure (1005 J·kg^{-1}·°C^{-1}), T is the 2-m air temperature (°C), L_v is the latent heat of vaporization (J·kg^{-1}), and q is the specific humidity (kg·kg^{-1}).

Here, q is calculated from 2-m dew point temperature (T_d, °C) and surface pressure (p, hPa) using the following equation[66]:

$$e = 6.112 \exp\left(\frac{17.67 T_d}{T_d + 243.5}\right) \tag{2}$$

$$q = \frac{0.622 e}{p - 0.378 e} \tag{3}$$

where e is the actual vapor pressure (hPa).

L_v is calculated as a linear function of T:

$$L_v = (2.501 - 0.00237 T) \times 10^6 \tag{4}$$

In addition, the relative humidity is calculated as the ratio of the e to the saturation vapor pressure (e_s, hPa)[67] as follows:

$$RH = 100 \times \frac{e}{e_s} \tag{5}$$

$$e_s = 6.112 \exp\left(\frac{17.67 T}{T + 243.5}\right) \tag{6}$$

Pairing of land grid cells and sea stations in coastal areas

In our study, heatwaves occur over land, while extreme sea levels are defined based on sea stations. To identify CHWESL events resulting from a combination of heatwaves and extreme sea levels, we paired land grid cells and sea stations using the following steps based on the minimum-distance method:

(1) We converted the shapefile of the global coastline to a raster file with a spatial resolution of 0.25° × 0.25°.
(2) For each grid cell in the raster file of the global coastline, we found the nearest land grid cell in the air temperature dataset based on the Euclidean distance.
(3) Since a land grid cell might have been assigned to multiple grid cells of coastlines, we removed duplicates. This results in a unique set of grid cell records for the coastal land grid cells.
(4) We assigned each land grid cell in the coastal areas to the nearest sea station in the ERA5 reanalysis dataset of total water level based on the Euclidean distance. The pairing of land grid cells and corresponding sea stations is what we define as the coastal areas.
(5) To conduct analyses of physical processes using sea-related atmospheric variables (i.e., 10-m wind and surface pressure), we assigned each sea station to the sea grid cell in these datasets (with a spatial resolution of 0.25° × 0.25°) that was closest to it.

After completing the pairing process, we identified 9492 land grid cells (Supplementary Fig. 1a). These land grid cells were paired with the nearest 9492 sea stations in the ERA5 reanalysis dataset of total water level and 9492 sea grid cells in the sea-related atmospheric variables dataset (i.e., surface pressure and 10-m wind). This pairing method results in a promising spatial proximity between the land grid cells and their corresponding paired sea stations (Supplementary Fig. 19). This allows us to investigate the risk of extreme sea levels for coastal communities threatened by heatwaves on the coast. The pairing of land grid cells and sea stations for the future simulation datasets was conducted in a similar way (Supplementary Fig. 20). All these steps were performed using Python 3.9.

Definition, metrics, and likelihood of extreme events

Definition. Although there is no universal definition for heatwaves and extreme sea levels, there are several criteria and thresholds that have been extensively used and tested in the literatures. We defined an event as a heatwave when the T_e is higher than a percentile-based threshold for at least three consecutive days[64]. The threshold refers to the 90th percentile of ranking T_e for the study period of 1979–2017 using a centered 15-day window (i.e., total samples are 39 years × 15 days = 585 days), following the previous study[68]. An extreme sea level event is considered when the W_t is higher than the 90th percentile threshold[69,70] of all the W_t records available for that station (i.e., total samples are 39 years × 365 days = 14,235 days). The 90th percentile threshold of W_t was determined by the fitted Generalized Extreme Value distribution (GEV), which is a commonly used method for estimating extreme sea level events[71,72]. We also performed a sensitivity analysis using different threshold levels (90th, 95th, and 99th percentiles) to identify heatwave and extreme sea level events (Supplementary Fig. 23), which could help inform risk management decisions on CHWESL events.

CHWESL events are defined as the concurrence of heatwaves and extreme sea levels during the extended summer season, which spans from May to September in the Northern Hemisphere and from November to March in the Southern Hemisphere. To identify a CHWESL day, we consider any day during a heatwave that is concurrent with any day of an extreme sea level event. A CHWESL event is defined as having at least one CHWESL day, and consecutive CHWESL days are combined into a single event. To separate adjacent events, we employed a window-based de-clustering method with a window size of three days[73].

Metrics. In this study, we used occurrence, total occurrence, and intensity to characterize extreme events. The occurrence is the number of days of extreme events within a year[74,75]. Total occurrence, as shown in Fig. 1a, refers to the sum of occurrences over multiple years. We quantified the intensity of a heatwave day as the percentile rank (ranging from the 90th to 99.5th percentile) of the T_e of that day. T_e is derived from 2-m air temperature and specific humidity. Therefore, a higher intensity indicates higher air temperature and higher specific humidity, corresponding to hotter and more humid conditions, respectively. Similarly,

we determined the intensity of an extreme sea level day as the percentile rank of the W_t of that day. The use of a percentile-based intensity enables more meaningful comparisons between grid cells, thereby facilitating their integration into a unified assessment framework.

Likelihood. We used the likelihood to describe the probability of CHWESL events. The likelihood of CHWESL events during heatwaves is defined as the ratio between the number of heatwave days that are concurrent with extreme sea levels (i.e., CHWESL events) and the total number of heatwave days. The likelihood of CHWESL events during extreme sea levels was calculated analogously.

Sensitivity of CHWESL events to the intensity of individual extremes

To further analyze the characteristics of heatwaves and extreme sea levels, we classified them into 20 different levels of intensity. We then calculated the likelihood of CHWESL events during heatwaves and extreme sea levels with varying intensities. This approach enables us to examine the sensitivity of the likelihood of CHWESL events to the intensities of individual extremes. The 20 intensity levels range from 90th percentile to 99.5th percentile with a 0.5th percentile interval. An intensity level of the 90th percentile represents T_e or W_t greater than or equal to the 90th percentile value but less than the 90.5th percentile value. In the sensitivity analysis, the likelihood of CHWESL events during heatwaves of a specific intensity is determined by calculating the ratio between the number of heatwave days concurrent with extreme sea levels (i.e., CHWESL events) and the total number of heatwave days at that specific intensity. We only consider the grid cells that experience CHWESL events during all heatwaves with 20 intensity levels. The likelihood of CHWESL events during extreme sea levels with a specific intensity was calculated analogously.

We used a linear least-squares regression analysis to examine the sensitivity of the likelihood of CHWESL events to the intensity of individual extremes. To assess the significance of the regression slope, we utilized the Wald test with a t-distribution to obtain a two-sided *p*-value. The null hypothesis assumed that the regression slope was zero, while the alternative hypothesis considered a non-zero slope.

In addition, we explored an alternative classification of intensity. We categorized the intensity into 10 levels, ranging from the 90th percentile to the 99th percentile, with a one percentile interval. This alternative classification did not alter the significance of our findings, as demonstrated in Supplementary Fig. 9.

Data availability

All data used in this study are publicly available. The ERA5 reanalysis data of 2-m air temperature and large-scale atmospheric variables are accessible through https://cds.climate.copernicus.eu/cdsapp#!/dataset/reanalysis-era5-single-levels?tab=overview and https://cds.climate.copernicus.eu/cdsapp#!/dataset/reanalysis-era5-pressure-levels?tab=overview. The CMIP6 model outputs of 2-m air temperature and specific humidity are available at https://cds.climate.copernicus.eu/cdsapp#!/dataset/projections-cmip6?tab=overview. The reanalysis data and CMIP6 model outputs of total water level are available at https://cds.climate.copernicus.eu/cdsapp#!/dataset/sis-water-level-change-timeseries-cmip6?tab=overview. The tide gauge observation of total water level is available at https://gesla787883612.wordpress.com/. The GSHHG data are accessible through https://www.soest.hawaii.edu/pwessel/gshhg/. The datasets used to reproduce the methods and findings of this study are available at https://doi.org/10.5281/zenodo.10532021.

Code availability

The code used for this study is available at https://doi.org/10.5281/zenodo.10532021.

Received: 9 August 2023; Accepted: 14 February 2024;
Published online: 11 April 2024

References

1. Fan, B. & Li, Y. Coupled land-sea warming dominates the net land carbon uptake variability in the Greater Bay Area of South China. *Earths Fut.* **10**, https://doi.org/10.1029/2021ef002556 (2022).
2. Weymer, B. A. et al. The coastal transition zone is an underexplored frontier in hydrology and geoscience. *Communications Earth Environ.* **3**, https://doi.org/10.1038/s43247-022-00655-8 (2022).
3. Seibert, S. L. et al. Investigating the land-sea transition zone. In: *Youmares 9 - the Oceans: Our Research, Our Future*, 225–242, https://doi.org/10.1007/978-3-030-20389-4_12 (2020).
4. Tebaldi, C. et al. Extreme sea levels at different global warming levels. *Nat. Clim. Change* **11**, 746, https://doi.org/10.1038/s41558-021-01127-1 (2021).
5. Rasmussen, D. J. et al. Extreme sea level implications of 1.5 degrees C, 2.0 degrees C, and 2.5 degrees C temperature stabilization targets in the 21st and 22nd centuries. *Environ. Res. Lett.* **13**, https://doi.org/10.1088/1748-9326/aaac87 (2018).
6. Wahl, T. et al. Understanding extreme sea levels for broad-scale coastal impact and adaptation analysis. *Nat. Commun.* **8**, 16075 (2017).
7. Philip, S. Y. et al. Rapid attribution analysis of the extraordinary heat wave on the pacific coast of the us and canada in june 2021. *Earth Syst. Dyn.* **13**, 1689–1713, (2022).
8. Clemesha, R. E. S., Guirguis, K., Gershunov, A., Small, I. J. & Tardy, A. California heat waves: Their spatial evolution, variation, and coastal modulation by low clouds. *Clim. Dyn.* **50**, 4285–4301, (2017).
9. Sharma, S. & Mujumdar, P. Increasing frequency and spatial extent of concurrent meteorological droughts and heatwaves in india. *Sci. Rep.* **7**, 15582, (2017).
10. Gershunov, A. & Guirguis, K. California heat waves in the present and future. *Geophys. Res. Lett.* **39**, https://doi.org/10.1029/2012gl052979 (2012).
11. Vicedo-Cabrera, A. M. et al. The burden of heat-related mortality attributable to recent human-induced climate change. *Nat. Clim. Change* **11**, 492–500, (2021).
12. Perkins, S. E., Alexander, L. V. & Nairn, J. R. Increasing frequency, intensity and duration of observed global heatwaves and warm spells. *Geophys. Res. Lett.* **39**, https://doi.org/10.1029/2012gl053361 (2012).
13. Domeisen, D. I. V. et al. Prediction and projection of heatwaves. *Nat. Rev. Earth Environ.* https://doi.org/10.1038/s43017-022-00371-z (2022).
14. Guirguis, K., Gershunov, A., Tardy, A. & Basu, R. The impact of recent heat waves on human health in california. *J. Appl. Meteorol. Climatol.* **53**, 3–19, (2014).
15. Arns, A. et al. Non-linear interaction modulates global extreme sea levels, coastal flood exposure, and impacts. *Nat. Commun.* **11**, 1918 (2020).
16. IPCC. Contribution of working group I to the sixth assessment report of the intergovernmental panel on climate change. In: *Climate Change 2021: The Physical Science Basis*, 2391. https://doi.org/10.1017/9781009157896 (2021).
17. Vousdoukas, M. I. et al. Global probabilistic projections of extreme sea levels show intensification of coastal flood hazard. *Nat. Commun.* **9**, 2360, (2018).
18. Hinkel, J. et al. Coastal flood damage and adaptation costs under 21st century sea-level rise. *Proc. Natl Acad. Sci.* **111**, 3292–3297, (2014).
19. MacManus, K., Balk, D., Engin, H., McGranahan, G. & Inman, R. Estimating population and urban areas at risk of coastal hazards, 1990-2015: How data choices matter. *Earth Syst. Sci. Data* **13**, 5747–5801, (2021).
20. Knox, P. *Alicante hit by 'mini-tsunami' caused by saharan heat surge with brit tourists facing 47°C sizzler* (The SUN, 2021). https://www.thesun.co.uk/news/worldnews/15840416/alicante-mini-tsunami-saharan-heat-surge-brits-facing-46c-sizzler/.

21. Peacock, A. *Alicante hit by mini-tsunami leaving parts of brit tourist hotspot under water* (Mirror, 2021). https://www.mirror.co.uk/news/uk-news/alicante-hit-meteotsunami-leaving-parts-24745448.
22. Seneviratne, S. I., et al. Contribution of working group I to the sixth assessment report of the intergovernmental panel on climate change. In: *Climate change 2021: the physical science basis* 1513–1766, https://doi.org/10.1017/9781009157896.013 (2021).
23. Muis, S. et al. A high-resolution global dataset of extreme sea levels, tides, and storm surges, including future projections. *Front. Marine Sci.* **7**, https://doi.org/10.3389/fmars.2020.00263 (2020).
24. Neumann, B., Vafeidis, A. T., Zimmermann, J. & Nicholls, R. J. Future coastal population growth and exposure to sea-level rise and coastal flooding-a global assessment. *PLoS One* **10**, e0118571, (2015).
25. Jones, B. & O'Neill, B. C. *Global one-eighth degree population base year and projection grids based on the shared socioeconomic pathways, revision 01* (NASA Socioeconomic Data and Applications Center (SEDAC), 2020). https://doi.org/10.7927/m30p-j498. Accessed 22-08-2022.
26. Barragán, J. M. & de Andrés, M. Analysis and trends of the world's coastal cities and agglomerations. *Ocean Coastal Manag.* **114**, 11–20, (2015).
27. You, J., Wang, S., Zhang, B., Raymond, C. & Matthews, T. Growing threats from swings between hot and wet extremes in a warmer world. *Geophys. Res. Lett.* **50**, https://doi.org/10.1029/2023gl104075 (2023).
28. Hendry, A. et al. Assessing the characteristics and drivers of compound flooding events around the uk coast. *Hydrol. Earth Syst. Sci.* **23**, 3117–3139, (2019).
29. Zscheischler, J. et al. A typology of compound weather and climate events. *Nat. Rev. Earth Environ.* **1**, 333–347, (2020).
30. Ha, K. J. et al. Dynamics and characteristics of dry and moist heatwaves over east asia. *Npj Clim. Atmos. Sci.* **5**, https://doi.org/10.1038/s41612-022-00272-4 (2022).
31. Chen, R. & Lu, R. Y. Comparisons of the circulation anomalies associated with extreme heat in different regions of eastern china. *J. Clim.* **28**, 5830–5844, (2015).
32. Needham, H. F., Keim, B. D. & Sathiaraj, D. A review of tropical cyclone-generated storm surges: Global data sources, observations, and impacts. *Rev. Geophys.* **53**, 545–591, (2015).
33. Gori, A., Lin, N., Xi, D. & Emanuel, K. Tropical cyclone climatology change greatly exacerbates us extreme rainfall–surge hazard. *Nat. Clim. Change* **12**, 171–178, (2022).
34. Lin, N., Emanuel, K., Oppenheimer, M. & Vanmarcke, E. Physically based assessment of hurricane surge threat under climate change. *Nat. Clim. Change* **2**, 462–467, (2012).
35. Muis, S., Verlaan, M., Winsemius, H. C., Aerts, J. C. & Ward, P. J. A global reanalysis of storm surges and extreme sea levels. *Nat. Commun.* **7**, 11969, (2016).
36. Wade, L. *How a melting ice sheet could actually lower sea level in some places* (*Science Magazine*, 2016).
37. Rogers, C. D. W. et al. Recent increases in exposure to extreme humid-heat events disproportionately affect populated regions. *Geophys. Res. Lett.* **48**, https://doi.org/10.1029/2021GL094183 (2021).
38. Speizer, S., Raymond, C., Ivanovich, C. & Horton, R. M. Concentrated and intensifying humid heat extremes in the ipcc ar6 regions. *Geophys. Res. Lett.* **49**, https://doi.org/10.1029/2021GL097261 (2022).
39. Wang, P. et al. Increasing compound hazards of tropical cyclones and heatwaves over southeastern coast of china under climate warming. *J. Clim.* **36**, 2243–2257, (2023).
40. Zhao, D. C., Lin, Y. L., Li, Y. L. & Gao, X. Y. An extreme heat event induced by typhoon lekima (2019) and its contributing factors. *J. Geophys. Res. Atmos.* **126**, https://doi.org/10.1029/2021JD034760 (2021).
41. Matthews, T., Wilby, R. L. & Murphy, C. An emerging tropical cyclone-deadly heat compound hazard. *Nat. Clim. Change* **9**, 602, (2019).
42. Davis, L., Gertler, P., Jarvis, S. & Wolfram, C. Air conditioning and global inequality. *Global Environ. Change* **69**, https://doi.org/10.1016/j.gloenvcha.2021.102299 (2021).
43. Pavanello, F. et al. Air-conditioning and the adaptation cooling deficit in emerging economies. *Nat. Commun.* **12**, 6460, (2021).
44. Panteli, M. & Mancarella, P. Influence of extreme weather and climate change on the resilience of power systems: Impacts and possible mitigation strategies. *Electric Power Syst. Res.* **127**, 259–270, (2015).
45. Biardeau, L. T., Davis, L. W., Gertler, P. & Wolfram, C. Heat exposure and global air conditioning. *Nat. Sustain.* **3**, 25–28, (2019).
46. Matthews, T. Humid heat and climate change. *Progr. Phys. Geogr. Earth Environ.* **42**, 391–405, https://doi.org/10.1177/0309133318776490 (2018).
47. Hooijer, A. & Vernimmen, R. Global lidar land elevation data reveal greatest sea-level rise vulnerability in the tropics. *Nat. Commun.* **12**, 3592, (2021).
48. CIA. *The 20 countries with the highest population growth rate in 2021 (compared to the previous year) [graph]* (Statista, 2022).
49. Jones, B. & O'Neill, B. C. Spatially explicit global population scenarios consistent with the shared socioeconomic pathways. *Environ. Res. Lett.* **11**, https://doi.org/10.1088/1748-9326/11/8/084003 (2016).
50. King, A. D. & Harrington, L. J. The inequality of climate change from 1.5 to 2°C of global warming. *Geophys. Res. Lett.* **45**, 5030–5033, https://doi.org/10.1029/2018gl078430 (2018).
51. Hersbach, H. et al. Era5 hourly data on single levels from 1959 to present [dataset]. In: *Copernicus Climate Change Service (C3S) Climate Data Store (CDS)*. https://doi.org/10.24381/cds.adbb2d47 (2018). Accessed on 01-01-2022.
52. Hersbach, H., et al. Era5 hourly data on pressure levels from 1959 to present [dataset]. In: *Copernicus Climate Change Service (C3S) Climate Data Store (CDS)*. https://doi.org/10.24381/cds.bd0915c6 (2018). Accessed on 01-01-2023.
53. Di Virgilio, G. et al. Selecting CMIP6 gcms for cordex dynamical downscaling: Model performance, independence, and climate change signals. *Earth Fut.* **10**, https://doi.org/10.1029/2021ef002625 (2022).
54. Copernicus Climate Change Service, C. D. S. CMIP6 climate projections [dataset]. In: *CMIP6 climate projections. Copernicus Climate Change Service (C3S) Climate Data Store (CDS)*. https://doi.org/10.24381/cds.c866074c (2022). Accessed 01-12-2022.
55. Sanne Muis, M. I. A., et al. Global sea level change time series from 1950 to 2050 derived from reanalysis and high resolution CMIP6 climate projections [dataset]. In *Copernicus Climate Change Service (C3S) Climate Data Store (CDS)*. https://doi.org/10.24381/cds.a6d42d60 (2022). Accessed 01-12-2022.
56. You, J. W. & Wang, S. Higher probability of occurrence of hotter and shorter heat waves followed by heavy rainfall. *Geophys. Res. Lett.* **48**, https://doi.org/10.1029/2021GL094831 (2021).
57. Chen, H. J. & Wang, S. Accelerated transition between dry and wet periods in a warming climate. *Geophys. Res. Lett.* **49**, https://doi.org/10.1029/2022GL099766 (2022).
58. Wessel, P. & Smith, W. H. F. A global, self-consistent, hierarchical, high-resolution shoreline database. *J. Geophys. Res. Solid Earth* **101**, 8741–8743, (1996).
59. Qiu, J., Liu, B., Yang, F., Wang, X. & He, X. Quantitative stress test of compound coastal-fluvial floods in china's pearl river delta. *Earth Fut.* **10**, https://doi.org/10.1029/2021ef002638 (2022).
60. Marsooli, R. & Lin, N. Numerical modeling of historical storm tides and waves and their interactions along the U.S. East and gulf coasts. *J. Geophys. Res. Oceans* **123**, 3844–3874, (2018).
61. Vousdoukas, M. I. et al. Sandy coastlines under threat of erosion. *Nat. Clim. Change* **10**, 260–263, https://doi.org/10.1038/s41558-020-0697-0 (2020).

62. IPCC. *Climate change 2013: The physical science basis. Contribution of working group I to the fifth assessment report of the intergovernmental panel on climate change*, 1535 (Cambridge University Press, 2013).
63. Burke, M., Davis, W. M. & Diffenbaugh, N. S. Large potential reduction in economic damages under un mitigation targets. *Nature* **557**, 549–553, (2018).
64. Rousi, E., Kornhuber, K., Beobide-Arsuaga, G., Luo, F. & Coumou, D. Accelerated western european heatwave trends linked to more-persistent double jets over eurasia. *Nat. Commun.* **13**, 3851, (2022).
65. Schoof, J. T., Heern, Z. A., Therrell, M. D. & Remo, J. W. F. Assessing trends in lower tropospheric heat content in the central United States using equivalent temperature. *Int J Climatol.* **35**, 2828–2836 (2015).
66. Bolton, D. The computation of equivalent potential temperature. *Monthly Weather Rev.* **108**, 1046–1053 (1980).
67. Lawrence, M. G. The relationship between relative humidity and the dewpoint temperature in moist air - a simple conversion and applications. *Bull. Am. Meteorol. Soc.* **86**, 225, (2005).
68. Perkins-Kirkpatrick, S. E. & Lewis, S. C. Increasing trends in regional heatwaves. *Nat. Commun.* **11**, 3357, (2020).
69. Wahl, T. & Chambers, D. P. Evidence for multidecadal variability in us extreme sea level records. *J. Geophys. Res. Oceans* **120**, 1527–1544, (2015).
70. Kirezci, E. et al. Projections of global-scale extreme sea levels and resulting episodic coastal flooding over the 21st century. *Sci. Rep.* **10**, 11629, (2020).
71. Rashid, M. M., Wahl, T., Chambers, D. P., Calafat, F. M. & Sweet, W. V. An extreme sea level indicator for the contiguous united states coastline. *Sci. Data* **6**, 326, (2019).
72. Menéndez, M., Méndez, F. J., Luceño, A. & Losada, I. J. Analyzing monthly extreme sea levels with a time-dependent gev model. *J. Atmos. Oceanic Technol.* **24**, 894–911, (2007).
73. Bevacqua, E. et al. Higher probability of compound flooding from precipitation and storm surge in europe under anthropogenic climate change. *Sci. Adv.* **5**, eaaw5531, (2019).
74. Nairn, J. R. & Fawcett, R. J. The excess heat factor: A metric for heatwave intensity and its use in classifying heatwave severity. *Int. J. Environ. Res. Public Health* **12**, 227–253, (2014).
75. Horton, D. E. et al. Contribution of changes in atmospheric circulation patterns to extreme temperature trends. *Nature* **522**, 465–469, (2015).

Acknowledgements

S.W. acknowledges support from the Environment and Conservation Fund (Grant P0038498) and the Hong Kong Polytechnic University (Grant P0036639, P0039238).

Author contributions

M.Z. and S.W. designed the study. M.Z. carried out the analysis and drafted the manuscript. S.W. supervised the analysis and contributed to the interpretation and discussion of the results. M.Z. and S.W. revised and edited the manuscript.

Competing interests

The authors declare no competing interests.

Additional information

Supplementary information The online version contains supplementary material available at https://doi.org/10.1038/s43247-024-01274-1.

Correspondence and requests for materials should be addressed to Shuo Wang.

Peer review information *Communications Earth & Environment* thanks Md Mamunur Rashid, Manal Elawady and the other, anonymous, reviewer(s) for their contribution to the peer review of this work. Primary Handling Editors: Jennifer Veitch and Aliénor Lavergne. A peer review file is available.